STABILITY OF THE NON-LINEAR SLIDER BEHAVIOR DUE TO DISK WAVINESS IN THE PRESENCE OF INTERMOLECULAR AND ELECTROSTATIC FORCES

Vineet Gupta and David B Bogy

Computer Mechanics Laboratory

Department of Mechanical Engineering

University of California

Berkeley, 94720

vineet@cml.me.berkeley.edu

November, 2005

ABSTRACT

In this paper we present a theoretical investigation of the stability and the dynamics of the non-linear behavior of a slider at very low head media spacing. A single DOF head disk interface (HDI) model, with constant air bearing stiffness and damping has been used to study the effect of disk waviness on the nonlinear slider dynamics in the presence of intermolecular and electrostatic forces. A variational approach based on the principle of least action was used to derive the equations of motion of the slider. Further, a stability criteria was derived that helped to better understand the instabilities that appear in the slider when it is flying in close proximity to the disk surface. Due to the nonlinear nature of the interaction between the slider and the disk, we observed some unexpected features of the motion of the slider. In particular the effects of the nonlinear interaction force, air bearing stiffness and damping on the instabilities of the periodic motions of the slider are discussed in detail using a frequency-response diagram.

TABLE OF CONTENTS

LIST OF FIGURES

7. Evolution of the resonance peak computed for three different values of air bearing stiffness: $k_1 = 5*10^6$ *N/m,* $k_2 = 2.5*10^6$ *N/m and* $k_3 = 1*10^6$ *N/m*. The resonance frequency (ω_o) for the three cases is given by $\sqrt{(k/m)}$. The numerical parameters are *D = 4nm, c = 0.1 N/m/sec,* $H = 8.9*10^{-20}$ *J, v = 0.3 volts, dxdy = 1000* μm^2.
8. Evolution of the resonance peak computed for three different values of air bearing damping: $c_1 = 0.2$ *N/m/sec,* $c_2 = 0.1$ *N/m/sec and* $c_3 = 0.055$ *N/m/sec*. The numerical parameters are *D = 4nm, k =* $2.5*10^6$ *N/m, H =* $8.9*10^{-20}$ *J, v = 0.3 volts, dxdy = 1000* μm^2.
9. Evolution of the resonance peak computed for three different values of the Hamakar constant: $H_1 = 2.7*10^{-19}$ *J,* $H_2 = 8.9*10^{-20}$ *J and* $H_3 = 2.9*10^{-20}$ *J.* The numerical parameters are *D = 3.8 nm, k =* $2.5*10^6$ *N/m, c = 0.1 N/m/sec, v = 0 volts, dxdy = 1000* μm^2.
10. Evolution of the resonance peak computed for three different values of potential difference between the slider and the disk: $v_1 = 0.5$ *volts,* $v_2 = 0.3$ *volts and* $v_3 = 0$ *volts.* The numerical parameters are *D = 3.4 nm, k =* $2.5*10^6$ *N/m, c = 0.1 N/m/sec, H =* $8.9*10^{-20}$ *J, dxdy = 1000* μm^2.
11. Variation of the amplitude as a function of the distance, i.e. the approach-retract curve. The numerical parameters are *k = 2.5*106 N/m, c = 0.1 N/m/sec, u = 0.9, H = 2.9*10-20 J, and v = 0.0 volts.* The curve exhibits a hysteretic cycle (ABCD) due to the nonlinear force that characterizes bifurcations from a mono-stable to a bi-stable state.

1. INTRODUCTION

The disk drive industry is continually faced with the demand for higher areal recording densities, faster data access speeds, higher reliability, and lower costs. The new industry goal is to achieve an areal recording density of 1 Tbit/in^2. This demand for higher areal density translates directly into a demand for higher track density and higher linear bit density, which in turn, requires significant reduction in the in-plane and out-of-plane vibrations of the magnetic head. In order to achieve the necessary higher linear bit density, the Wallace spacing law dictates that the magnetic spacing between the slider and the disk must be reduced to less than 10 nm. At such low head disk spacing additional forces, such as intermolecular and electrostatic forces, will come into play, which may result in larger fly height modulations. A study of the effect of intermolecular and electrostatic forces on slider dynamics was presented in previous papers [1-3]. Besides, Wu and Bogy [4] have also shown that there is a reduction in fly height due to intermolecular forces (IMF) for sub 5nm flying sliders. Thornton and Bogy [5] also predicted instability due to these forces at the HDI. Here we extend our analysis and focus on the effect of disk waviness on the stability and dynamics of slider in the presence of intermolecular and electrostatic forces.

2. HEAD-DISK INTERFACE MODEL

The differential equation that describes the 1-dimentional motion $z(t)$ of the slider is given by

$$m\frac{d^2z(t)}{dt^2} + c\frac{dz(t)}{dt} + k\,z(t) = F_{disk}\cos(\omega t) - \nabla V[z(t)] \qquad (1)$$

where m, c and $k = m\omega_o^2$ are respectively the slider mass *(1.6 mg)*, air bearing damping and air bearing stiffness respectively and ω_o is the resonance frequency. $F_{disk}cos(\omega t)$ is the force due to disk waviness where $F_{disk} = k*a_{disk}$. Here ω is the disk waviness frequency and a_{disk} is the amplitude of disk waviness. *V[z(t)]* is the interaction potential due to intermolecular and electrostatic forces between the slider and the disk. To describe the interaction between the slider and the disk, the attractive coupling force is assumed to be derived from a plane-plane interaction and it can be expressed as [6]:

$$V[z(t)] = -\frac{H\,dxdy}{12\pi(D+z)^2} - \frac{\varepsilon_0\,k_e\,v^2\,dxdy}{2(D+z)} \qquad (2)$$

where H, ε_o, k_e, v, $dxdy$ and D are the Hamaker constant, permittivity constant (8.85 x 10^{-12} farad/m), dielectric constant of the medium (1 for air), potential difference between the slider and the disk, area of the slider in close proximity with the disk and the distance between the disk and the equilibrium position of the slider, respectively.

3. EULER-LAGRANGE EQUATIONS OF MOTION OF THE SLIDER

A variational method based on the principal of least action is used in this analysis. Instead of using canonical variables, which requires the use of Hamiltonians, Sturrock developed a technique that does not require canonical variables. It consists of averaging the Lagrangian and then writing down the corresponding Euler-Lagrange equations. Whitham developed a similar

technique for waves in which the frequency and wave number as well as the amplitude are slowly varying functions of space and time. Bispop supplied a more rigorous justification of this technique. Although this technique is not as elegant as those using canonical variables, it has the advantage of being directly applicable to partial as well as ordinary differential equations [7-12].

For any path $z(t)$, that could take the system from initial time t_a to final time t_b, we define an action $I[z(t)]$ which is a functional of the path $z(t)$ as:

$$I[z(t)] = \int_{t_a}^{t_b} L(z, \dot{z}, t)dt \tag{3}$$

Here L is the Lagrangian of the system given by:

$$L(z, \dot{z}, t) = T - U + W = \frac{1}{2} m \dot{z}(t)^2 - \left[\frac{1}{2} k\, z(t)^2 - z(t) F_{disk} \cos(\omega t) + V[z(t)] \right] - c\, z(t)\, \dot{z}(t) \tag{4}$$

The main aim of the use of the variational principal is to employ a harmonic trial function of the form $z(t) = A(t)\cos(\omega t+\varphi(t))$ that allows us to perform a non-perturbative analytical treatment in which the dissipation is included. Amplitude ($A(t)$) and phase ($\varphi(t)$) are assumed to be slowly varying functions with time compared to the period $T = 2\pi/\omega$. Since the oscillator responds with a delay to the excitation, the sign of the phase chosen means that φ varies in the domain [-180^o, 0^o]. To get the equations of motion in terms of amplitude and phase, we assume a long duration $\Delta t = t_b - t_a$ such that $\Delta t >> T$ and calculate the action as a sum of small pieces of duration T as:

$$I = \sum_n \int_{nT}^{(n+1)T} L(z, \dot{z}, t)dt = \sum_n \left(\frac{1}{T} \int_{nT}^{(n+1)T} L(z, \dot{z}, t)dt \right) T = \sum_n L_e T \tag{5}$$

Here L_e is the mean Lagrangian during one period and appears as an effective Lagrangian for a large time scale compared to the period. Owing to the quasi-stationary behavior of the amplitude and the phase over the period, the effective Lagrangian is calculated as follows:

$$L_e(A, \dot{A}, \varphi, \dot{\varphi}) = \frac{1}{T} \int_{nT}^{(n+1)T} L(z, \dot{z}, t) dt \tag{6}$$

Note that the effective Lagrangian is now a function of the new generalized coordinates A and φ and their associated generalized derivatives. Since the period T is small in comparison to $\Delta t = t_b - t_a$ during which the total action is evaluated, the continuous expression of the action is:

$$I = \int_{t_a}^{t_b} L_e(A, \dot{A}, \varphi, \dot{\varphi}) d\tau \tag{7}$$

where the measure $d\tau$ is such that $T << d\tau << \Delta t$.

The observation that the solution of the Lagrange's equations of motion extremizes the action was made by Hamilton. Jacobi extended Hamilton's work and stated that the equations of motion can be obtained using the (Jacobi's) Principle of Least or Stationary Action. It states that "*The motion of the particle on the configuration manifold is such that the path of the particle is geodesic with respect to the action-line element*" [7-12]. By definition, a geodesic curve between the two points is the path of shortest length between them. Expressed as a variational principle, the Euler-Lagrange necessary condition for the curve to be a geodesic is $\delta I = 0$.

Applying the principle of least action $\delta I = 0$ to the functional L_e, we obtain the Euler-Lagrange Equation for the effective Lagrangian:

$$\frac{d}{d\tau}\left(\frac{\partial L_e}{\partial \dot{A}}\right)-\left(\frac{\partial L_e}{\partial A}\right)=0$$
$$\frac{d}{d\tau}\left(\frac{\partial L_e}{\partial \dot{\varphi}}\right)-\left(\frac{\partial L_e}{\partial \varphi}\right)=0 \qquad (8)$$

Substituting the value of the effective Lagrangian calculated above in the Euler-Lagrange Equation of motion, we obtain:

$$\ddot{A}=\left[(\omega+\dot{\varphi})^2-\omega_o^2\right]A-\frac{c}{m}\dot{A}+\frac{F_{disk}}{m}\cos(\varphi)+\frac{H\,dxdy}{12\pi}\frac{6AD}{m(D^2-A^2)^{5/2}}+\frac{\varepsilon_o k_e v^2\,dxdy}{2}\frac{2A}{m(D^2-A^2)^{3/2}}$$
$$\ddot{\varphi}=-\left(\frac{2\dot{A}}{A}+\frac{c}{m}\right)(\omega+\dot{\varphi})-\frac{F_{disk}}{mA}\sin(\varphi) \qquad (9)$$

The equations of motion of the stationary solutions A and φ are then obtained by setting the first and second derivates of A and φ to be zero. Thus, we obtain two coupled equations in A and φ, expressed as:

$$\cos(\varphi)=\frac{A}{F_{disk}}\left(k-m\omega^2\right)-\frac{H\,D\,A\,dxdy}{2\pi F_{disk}(D^2-A^2)^{5/2}}-\frac{A\,\varepsilon_0\,k_e\,v^2\,dxdy}{F_{disk}(D^2-A^2)^{3/2}}$$
$$\sin(\varphi)=-\frac{c\,\omega\,A}{F_{disk}} \qquad (10)$$

Using the trigonometric identity $sin^2(\varphi) + cos^2(\varphi) = 1$, and rearranging the terms to get the relationship between the frequency and the amplitude at a given distance D, we get:

$$u_{\pm}(A)=\sqrt{\frac{F_{disk}^2\omega_o^2}{A^2c^2}-\frac{c^2}{4km}\left(1\mp\sqrt{1-\frac{4km}{c^2}\left(1-\frac{F_{disk}^2\omega_o^2}{A^2c^2}-\frac{H\,D\,dxdy}{2\pi k(D^2-A^2)^{5/2}}-\frac{\varepsilon_o k_e v^2\,dxdy}{k(D^2-A^2)^{3/2}}\right)}\right)^2} \qquad (11)$$

where $u = \omega/\omega_o$ is the driving frequency normalized to the resonance frequency of the free slider. Here the signs plus and minus are deduced from the sign of $cos(\varphi)$, u_- corresponds to the value of the phase ranging from 0^o to -90^o as $cos(\varphi) > 0$, and u_+ corresponds to the value of the phase

ranging from -90^o to -180^o as $cos(\varphi) < 0$. This is in agreement with the sign convention of the phase of the assumed harmonic solution of the form $z(t) = A(t)cos(\omega t+\varphi(t)$. The two branches define the distortion of the resonance peaks as a function of D, where u_- and u_+ gives the evolution of the resonance peak for frequency values below and above the resonance, respectively.

Fig.1 shows the distortion of the resonance peak versus the distance D. Red lines (-□-) correspond to u_- and blue lines (-○-) correspond to u_+. We observe that for an attractive force the peak is increasingly distorted towards the low frequencies as D is reduced. This is because for large values of D, the slider is far from the disk surface, and hence the nonlinear effects, i.e. the effect of intermolecular forces and electrostatic forces, are negligible and the peak keeps the well defined Lorenzian shape ($H = 0$ *and* $v = 0$). But at low separations the magnitude of the attractive forces increases, which results in the distortion of the resonance peak.

4. HEAD DISK INTERFACE STABILITY CRITERIA

To obtain the stability criteria of the branches u_+ and u_- of the resonance peaks, the equations must be linearized about the stationary solutions (now identified by index '*eq*') [13-18]. We assume that $A = A_{eq} + A_p$ and $\varphi = \varphi_{eq} + \varphi_p$ where A_p and φ_p are small perturbations from equilibrium points A_{eq} and φ_{eq} respectively. On linearization the equations of motion (9) can be written in the state space form as:

$$\frac{d}{dt}\begin{pmatrix} A_p \\ \varphi_p \\ \dot{A}_p \\ \dot{\varphi}_p \end{pmatrix} = M \begin{pmatrix} A_p \\ \varphi_p \\ \dot{A}_p \\ \dot{\varphi}_p \end{pmatrix}$$

where,

$$M = \begin{pmatrix} 0 & 0 & 1 & 0 \\ 0 & 0 & 0 & 1 \\ \omega^2 - \omega_o^2 + \Delta & c\omega A_{eq}/m & -c/m & 2\omega A_{eq} \\ -c\omega/mA_{eq} & -\cos(\varphi_s)F_{disk}/mA_{eq} & -2\omega/A_{eq} & -c/m \end{pmatrix} \tag{12}$$

$$with \quad \Delta = \frac{H\,dxdy}{12\pi}\left(\frac{6D}{m(D^2-A^2)^{5/2}} + \frac{30A^2D}{m(D^2-A^2)^{7/2}}\right) + \frac{\varepsilon_o k_e v^2\,dxdy}{2}\left(\frac{2}{m(D^2-A^2)^{3/2}} + \frac{6A^2}{m(D^2-A^2)^{5/2}}\right)$$

To discuss the stability of the branches, we calculate the eigenvalues of the matrix *M* as *det(M-λI) = 0*. This equation reduces to the form:

$$\left(\lambda^2 + c\lambda/m + \mathrm{X}\right)\left(\lambda^2 + c\lambda/m + \mathrm{Y}\right) = 0$$

where,

$$X + Y = 3\omega^2 + \omega_o^2 - \Delta + \frac{F_{disk}\cos(\varphi_{eq})}{mA_{eq}} \tag{13}$$

$$XY = \left(\frac{c\omega}{m}\right)^2 - \left(\omega^2 - \omega_o^2 + \Delta\right)\frac{F_{disk}\cos(\varphi_{eq})}{mA_{eq}}$$

The characteristic equation is equivalent to the following system:

$$\begin{aligned} &\lambda^2 + c\lambda/m + X = 0 && \lambda^2 + c\lambda/m + Y = 0 \\ &\Rightarrow \lambda_{1,2} = \left(-c/m \pm \sqrt{(c/m)^2 - 4X}\right)/2 && \Rightarrow \lambda_{3,4} = \left(-c/m \pm \sqrt{(c/m)^2 - 4Y}\right)/2 \end{aligned} \tag{14}$$

The stable solutions are those given by $R_e(\lambda_i) < 0$, thus:

$$c/m > \sqrt{(c/m)^2 - 4X} \quad and \quad c/m > \sqrt{(c/m)^2 - 4Y}$$
$$\Rightarrow X > 0 \quad and \quad Y > 0 \tag{15}$$

The condition $X > 0$ and $Y > 0$ is equivalent to saying that $X+Y > 0$ and $XY > 0$.

We first consider the term $XY > 0$. Observe that,

$$\frac{A_{eq}}{F_{disk}}\left(k - m\omega^2\right) - \tilde{\Lambda} = \cos(\varphi_{eq}) = \pm\sqrt{1 - \sin^2(\varphi_{eq})} = \pm\sqrt{1 - \left(\frac{c\,\omega\,A_{eq}}{F_{disk}}\right)^2}$$
$$where \quad \tilde{\Lambda} = \frac{H\,D\,A_{eq}\,dxdy}{2\pi F_{disk}(D^2 - A_{eq}^2)^{5/2}} - \frac{A_{eq}\,\varepsilon_0\,k_e\,v^2\,dxdy}{F_{disk}(D^2 - A_{eq}^2)^{3/2}} \tag{16}$$

Next, we define a function $R(A_{eq},\omega)$ as:

$$R(A_{eq},\omega) = \frac{A_{eq}}{F_{disk}}\left(k - m\omega^2\right) - \frac{H\,D\,A_{eq}\,dxdy}{2\pi F_{disk}(D^2 - A_{eq}^2)^{5/2}} - \frac{A_{eq}\,\varepsilon_0\,k_e\,v^2\,dxdy}{F_{disk}(D^2 - A_{eq}^2)^{3/2}} \mp \sqrt{1 - \left(\frac{c\,\omega\,A_{eq}}{F_{disk}}\right)^2} = 0 \tag{17}$$

Therefore,

$$dR(A_{eq},\omega) = \partial_{A_{eq}} R(A_{eq},\omega)dA_{eq} + \partial_{\omega} R(A_{eq},\omega)d\omega = 0 \tag{18}$$

and so,

$$\frac{dA_{eq}}{d\omega} = -\frac{\partial_{\omega} R(A_{eq},\omega)}{\partial_{A_{eq}} R(A_{eq},\omega)} \tag{19}$$

Substituting the value of $R(A_{eq},\omega)$ in the above equations we get:

$$\frac{dA_{eq}}{d\omega} = \frac{2\omega F_{disk}}{m} \frac{\cos(\varphi_{eq}) - \dfrac{c^2 A_{eq}}{2mF_{disk}}}{\left(\dfrac{c\omega}{m}\right)^2 - \left(\omega^2 - \omega_o^2 + \Delta\right)\dfrac{F_{disk}\cos(\varphi_{eq})}{mA_{eq}}} \tag{20}$$

Note that the denominator is the product *XY*, thus:

$$XY > 0 \;\Leftrightarrow\; \frac{2\omega F_{disk}}{m} \frac{\cos(\varphi_{eq}) - \dfrac{c^2 A_{eq}}{2mF_{disk}}}{\dfrac{dA_{eq}}{d\omega}} > 0 \tag{21}$$

Since $2\omega F_{disk}/m$ is always positive, the stability condition $XY > 0$ reduces to:

$$\frac{\cos(\varphi_{eq}) - \dfrac{c^2 A_{eq}}{2mF_{disk}}}{\dfrac{dA_{eq}}{d\omega}} > 0 \tag{22}$$

Hence the stability criteria are:

$$\begin{aligned} &\frac{dA_{eq}}{d\omega} > 0 \quad and \quad \cos(\varphi_{eq}) > \frac{c^2 A_{eq}}{2mF_{disk}} \\ &or, \quad \frac{dA_{eq}}{d\omega} < 0 \quad and \quad \cos(\varphi_{eq}) < \frac{c^2 A_{eq}}{2mF_{disk}} \end{aligned} \tag{23}$$

Next we consider the condition $X+Y > 0$. For the range of values that the parameters can take it turns out always to be that

$$X + Y = 3\omega^2 + \omega_o^2 - \Delta + \frac{F_{disk}\cos(\varphi_{eq})}{mA_{eq}} > 0\,. \tag{24}$$

Hence the stability criteria's are only given by the condition $XY > 0$.

Fig's. 2 and 3 show the distortion of the resonance peak and of the associated phase curves, respectively. Fig's. 4 and 5 are the zooms on the region *'p'* of Fig. 2 and 3, respectively. From

Fig. 2 we observe that dA_{eq}/du_{+} is always negative for the branch u_{+} and from Fig. 3 we observe that the associated value of the phase is always below -90^{o}, thus $cos(\varphi_{eq}) < 0$ for the branch u_{+}. This analysis shows that u_{+} is always stable for all values of A_{eq}.

From Fig. 3 we observe that the phase associated with the branch u$_{-}$ is always above -90^{o}, thus $cos(\varphi_{eq}) > 0$ for the branch u_{-}. Thus for stability dA_{eq}/du_{-} must be > 0. From Fig. 2 we observe that the sign of derivative changes twice for the branch u_{-}. On the lower part of the branch corresponding to the small values of A, we observe that $dA_{eq}/du_{-} > 0$, which indicates that the branch is locally stable. When $dA_{eq}/du_{-} < 0$, the stability criteria is no longer satisfied and the branch u_{-} becomes unstable locally. On the upper part of the branch u_{-} the derivative changes sign again and dA_{eq}/du_{-} becomes positive, this implies that the branch u_{-} becomes stable again locally. Thus we see that the branch u_{-} and φ_{-} exhibit two stable and one unstable domain. The resonance condition is $dA_{eq}/du = 0$, which implies that $cos(\varphi_{eq}) = c^{2}A_{eq}/2mF_{disk}$. This condition can be used to say that $u_{-} = u_{+}$ and $\varphi_{-} = \varphi_{+}$ at the resonance.

5. RESULTS

5.1 EFFECT OF SLIDER-DISK SEPARATION ON HEAD-DISK INTERFACE STABILITY

Fig.6 plots the evolution of the resonance peak as the head disk separation varies. The evolution of the resonance peak is plotted for four different values of head disk separation: $D_1=10nm$, $D_2=5nm$, $D_3=3.5nm$ and $D_4=3.2nm$. We observe that for an attractive force, the peak is

increasingly distorted towards the low frequencies as D is reduced, which results in an increase in the width of the unstable regime. This is because as the head disk spacing reduces the magnitudes of intermolecular forces and electrostatic forces become increasingly significant and results in head-disk interface instability.

5.2 EFFECT OF AIR-BEARING STIFFNESS AND DAMPING ON THE HEAD-DISK INTERFACE STABILITY

Fig. 7 plots the variation of the frequency response curve for three different values of air bearing stiffness. We observe that as the air bearing stiffness increases the amplitude of slider vibration increases. There is also an increase in the unstable domain of u with an increase in the air bearing stiffness. Fig. 8 plots the variation of the frequency response curve for three different values of air bearing damping. In the absence of damping, the peak amplitude of slider vibration is infinite. We observe that as the air bearing damping increases the amplitude of slider vibration decreases. The unstable domain of u also decreases as the air bearing damping increases.

5.3 EFFECT OF INTERMOLECULAR FORCES AND ELECTROSTATIC FORCES ON HEAD-DISK INTERFACE STABILITY

Typical value of the Hamaker constant with a representative thickness of DLC layer on the slider and lubricant layer on the disk is $8.9*10^{-20}$ *J.* Similarly typical values of the Hamaker constant for a DLC-DLC interface and a Lube-Lube interface are $2.7*10^{-19}$ *J and* $2.9*10^{-20}$ *J* respectively. Fig. 9 plots the variation of the frequency response curve for three different values of the

Hamaker constant. As expected in the absence or for small magnitudes of intermolecular forces the peak keeps the well defined Lorenzian shape ($H = 0$ *and* $v = 0$). As the Hamaker constant increases, the magnitude of the intermolecular forces between the slider and the disk increases and this results in an increase in the amplitude of slider vibrations. There is also an increase in the unstable domain of u, with an increase in the magnitude of intermolecular forces. Fig. 10 plots the variation of the frequency response curve for three different values of potential difference between the slider and the disk. As the potential difference between the slider and the disk increases, the magnitude of electrostatic forces between the slider and the disk increases, which results in an increase in the amplitude of slider vibrations. There is also an increase in the unstable domain of u, with an increase in the magnitude of intermolecular forces.

5.4 APPROACH-RETRACT CURVES FOR SLIDER MOTION IN HDD

The multivaluedness of the approach-retract curve as shown in Fig. 11, due to the nonlinearity, has significance from the physical point of view because it leads to jump phenomena. We observe that the solution generates a domain of distance D where the slider may show unstable behavior. In the domain ABCD three values of the amplitude can be reached for a given value of the slider-disk separation. When the slider approaches the disk, the amplitude slowly increases up to point ‘D’ and then jumps to point ‘A’. At this point a further decrease in the distance between the slider and the disk results in the decrease of the amplitude. Similarly, when the slider is retracted from the disk, first the amplitude increase up to the point ‘B’ and then it jumps to point ‘C’. A further increase in the distance between the slider and the disk will result in a decrease in the amplitude. Analysis similar to that used in the case of the response diagram can

be used to predict the stability of the branches D_+ and D_-. We observe that the branch D_- is always stable. The stability of the branch D_+ depends on the value of *H and v*.

6. CONCLUSIONS

A theoretical analysis has been presented to investigate the stability of the slider in hard disk drives at the head disk interface (HDI). A single DOF HDI model, with constant air bearing stiffness and damping has been used to study the effect of disk waviness on the nonlinear slider dynamics in the presence of intermolecular and electrostatic forces. A variational approach based on the principle of least action was used in this analysis. The stationery solutions were obtained and a stability criterion was formulated in terms of the phase value and the sign of the derivative of the curve. This helped us to better understand the instabilities that appear in the slider when it is flying in close proximity to the disk surface. Due to the nonlinear nature of the interaction between the slider and the disk, we observed some unexpected features of the motion of the slider. We found that the branch associated to the disk waviness frequencies larger than the resonance frequency is always stable and the branch associated to the disk waviness frequencies smaller than the resonance frequency exhibits two stable domains and one unstable domain. In particular the effects of the nonlinear interaction force, air bearing stiffness and damping on the instabilities of the periodic motions of the slider are discussed in detail using the frequency-response diagram. We also found that as the magnitude of intermolecular and/or electrostatic forces increases, the system becomes increasingly unstable.

7. ACKNOWLEDGMENTS

This work was supported by the Computer Mechanics Laboratory at the University of California, Berkeley and Information Storage Industry Consortium's EHDR program.

8. REFERENCES

[1.] V. Gupta, and D.B. Bogy, "Effect of Intermolecular Forces on the Static and Dynamic Performance of Air Bearing Sliders: Part I – Effect of initial excitation and slider form factor on the stability," *ASME Journal of Tribology* (accepted for publication).

[2.] V. Gupta, and D.B. Bogy, "Effect of Intermolecular Forces on the Static and Dynamic Performance of Air Bearing Sliders: Part II – Dependence of the stability on the Hamaker constant, suspension preload and pitch angle," *ASME Journal of Tribology* (accepted for publication).

[3.] V. Gupta, and D.B. Bogy, "Dynamics of Sub-5nm Air Bearing Sliders in the Presence of Electrostatic and Intermolecular Forces at the Head Disk Interface," *IEEE Journal of Magnetics*, 41(2), 610-615, 2005.

[4.] L. Wu., "Physical modeling and numerical simulations of the slider air bearing problems in hard disk drives," Ph.D. dissertation, University of California, Berkeley,2001

[5.] B.H. Thornton, "Head-Disk Interface Dynamics of Ultra-Low Flying Air Bearing Sliders for Hard-Disk Drive Applications," Ph.D. dissertation, University of California, Berkeley, 2003

[6.] J. N. Israelachvili, Intermolecular and surface forces, 2nd ed. Academic Press, 1992.

[7.] H. Goldstein, Classical Mechanics, 2nd ed. Addison-Wesley, 1980.

[8.] V.I. Arnold, Mathematical Methods of Classical Mechanics, 2nd ed. Springer-Verlag, 1989.

[9.] J.E. Marsden, and T.S.Ratiu, Introduction to Mechanics and Symmetry: A Basic Exposition of Classical Mechanical Systems, Springer-Verlag, 1994.

[10.] E.T. Whittaker, Analytical Dynamics, 4th ed. Cambridge University Press, 1959.

[11.] E.T. Whittaker, A Treatise on the Analytical Dynamics of Particles and Rigid Bodies: With an Introduction to the Problem of Three Bodies, Dover, 1944.

[12.] L.A. Pars, A Treatise on Analytical Dynamics, Wiley, 1965.

[13.] E.J. Hinch, Perturbation Methods, Cambridge University Press, 1991.

[14.] J. Guckenheimer, and P. Holmes, Nonlinear Oscillations, Dynamical Systems, and Bifurcations of Vector Fields, Springer, 1991.

[15.] A.H. Nayfeh, and D.T. Mook, Nonlinear Oscillations, Wiley, 1995.

[16.] L. Meirovitch, Principles and Techniques of Vibrations, Prentice Hall, 1997.

[17.] J.K. Hale, and H. Kocak, Dynamics and Bifurcations, Springer-Verlag, 1991.

[18.] S. Wiggins, Introduction to Applied Nonlinear Dynamical Systems and Chaos, Springer, 2003.

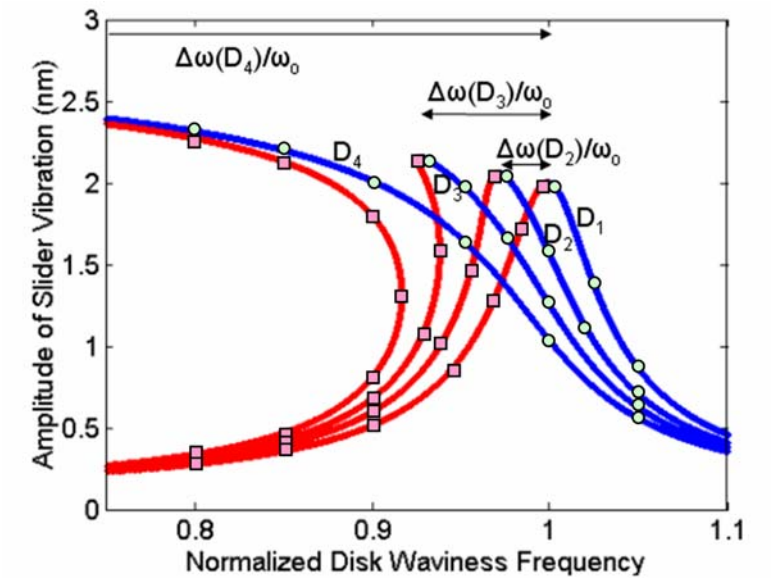

Fig.1 Evolution of the resonance peak computed for four different values of distance: D_1=10nm, D_2=5nm, D_3=3.5nm and D_4=3.2nm. Red lines (-□-) correspond to u_- and blue lines (-○-) correspond to u_+. The numerical parameters are $k = 2.5*10^6$ N/m, $c = 0.1$ N/m/sec, $H = 8.9*10^{-20}$ J, $v = 0.3$ volts, $dxdy = 1000\ \mu m^2$.

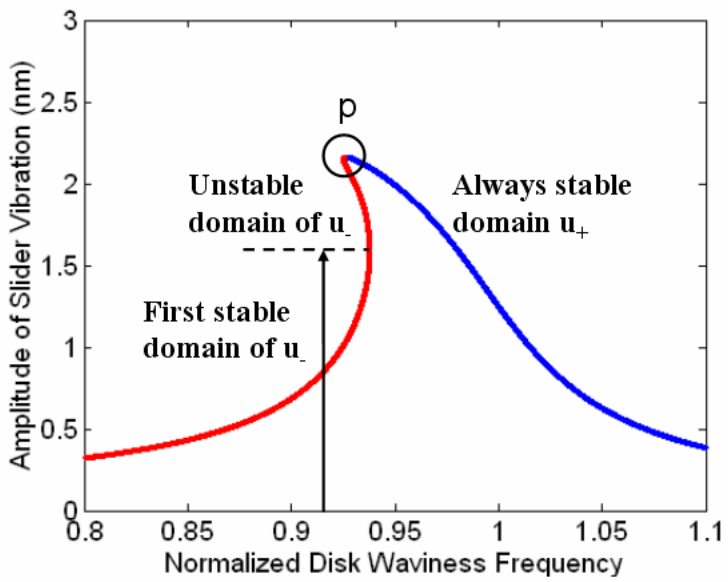

Fig.2 Evolution of the resonance peak computed for numerical values of $D=3.4nm$, $k = 2.5*10^{6}$ N/m, $c = 0.1$ $N/m/sec$, $H = 8.9*10^{-20}$ J, $v = 0.3$ $volts$, $dxdy = 1000$ μm^{2}. The stability criterion predicts that u_{+} is always stable, whereas u_{-} exhibits two stable domains and one unstable domain. The domains are separated by the points where the derivative $dA/du_{-} \rightarrow \pm\infty$.

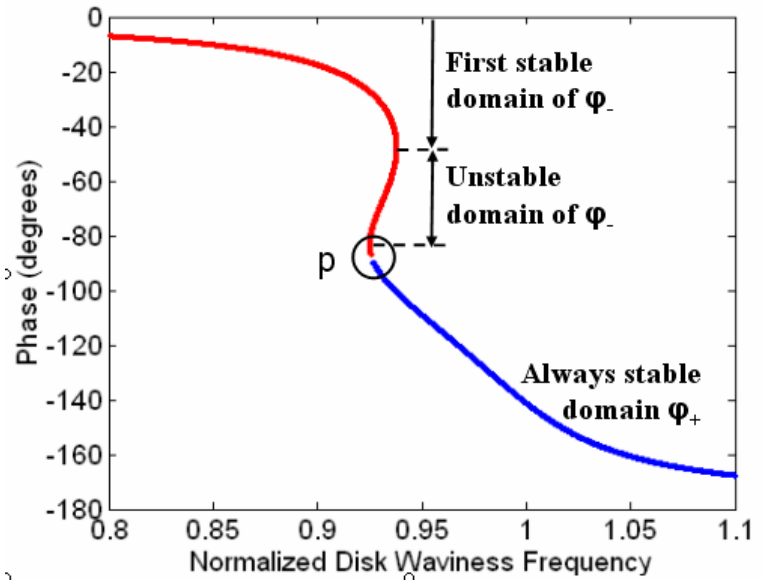

Fig.3 Evolution of the phase curve associated to the resonance peak plotted in Fig. 2 for the numerical value of $D=3.4nm$, $k = 2.5*10^{6}$ N/m, $c = 0.1$ $N/m/sec$, $H = 8.9*10^{-20}$ J, $v = 0.3$ $volts$, $dxdy = 1000\ \mu m^{2}$. The stability criterion predicts that φ_{+} is always stable, whereas φ_{-} exhibits two stable domains and one unstable domain.

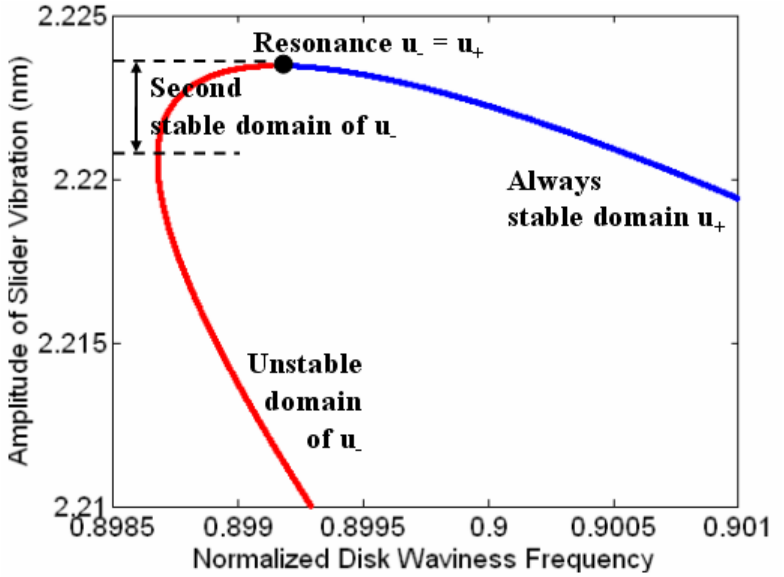

Fig.4 Zoom of the region '*p*' of the resonance peak shown in Fig.2. As dA/du_- diverges again, this defines a new domain u_- which is predicted to be stable. The resonance occurs where $u_+ = u_-$.

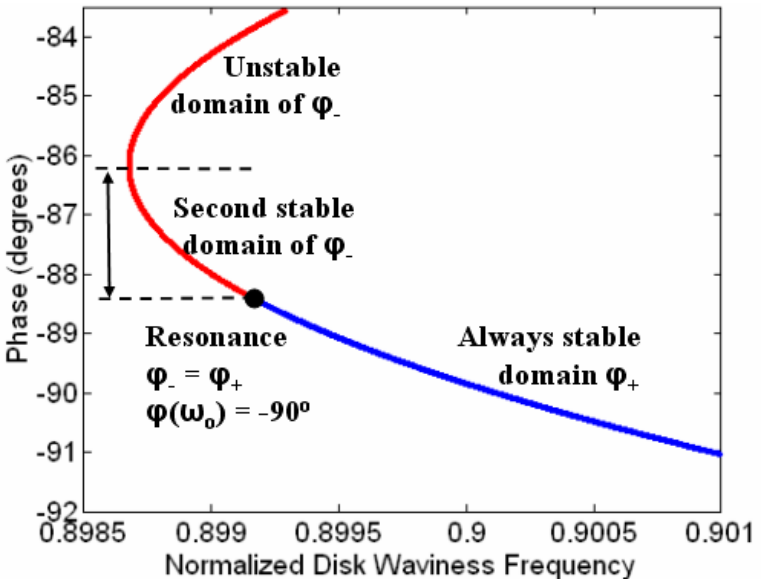

Fig.5 Zoom of the region '*p*' of the phase curve shown in Fig.3. The resonance is located at $\varphi = -90^{o}$ where $\varphi_{+} = \varphi_{-}$ and belongs to a stable domain.

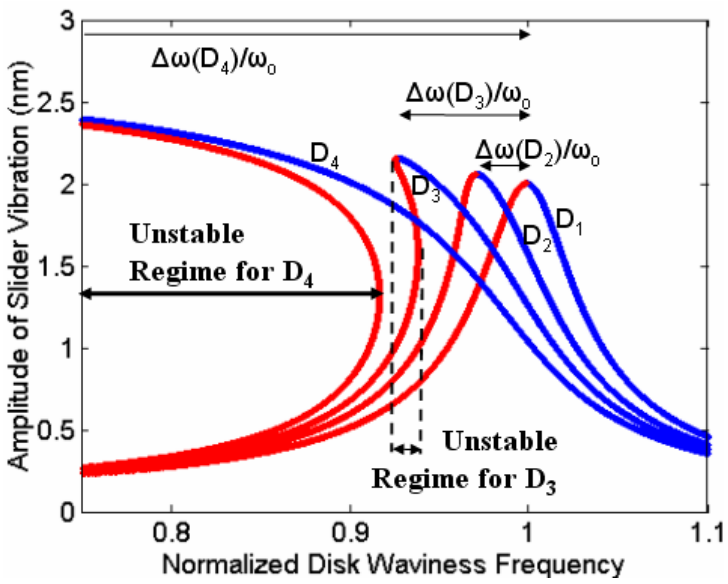

Fig.6 Evolution of the resonance peak computed for four different values of distance: D_1=10nm, D_2=5nm, D_3=3.5nm and D_4=3.2nm. The numerical parameters are $k = 2.5*10^6$ N/m, $c = 0.1$ N/m/sec, $H = 8.9*10^{-20}$ J, $v = 0.3$ volts, $dxdy = 1000\ \mu m^2$.

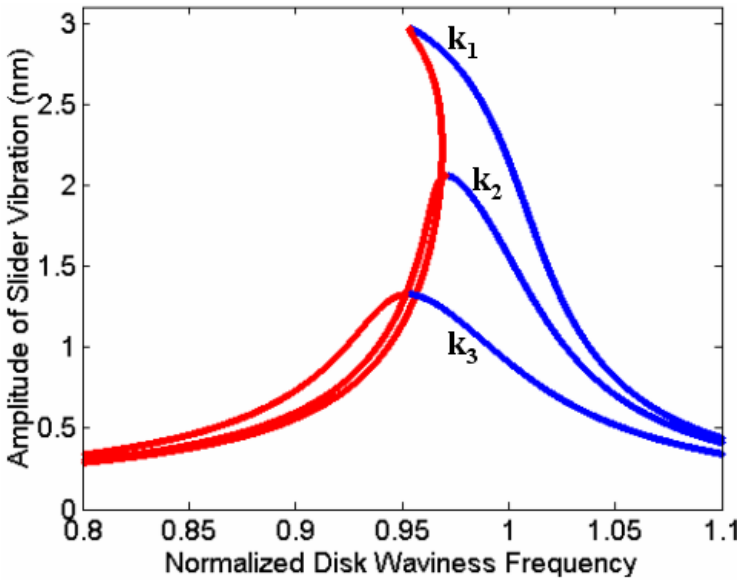

Fig.7 Evolution of the resonance peak computed for three different values of air bearing stiffness: $k_1 = 5*10^6$ *N/m,* $k_2 = 2.5*10^6$ *N/m and* $k_3 = 1*10^6$ *N/m*. The resonance frequency (ω_o) for the three cases is given by $\sqrt{(k/m)}$. The numerical parameters are *D = 4nm, c = 0.1 N/m/sec,* $H = 8.9*10^{-20}$ *J, v = 0.3 volts, dxdy = 1000* μm^2.

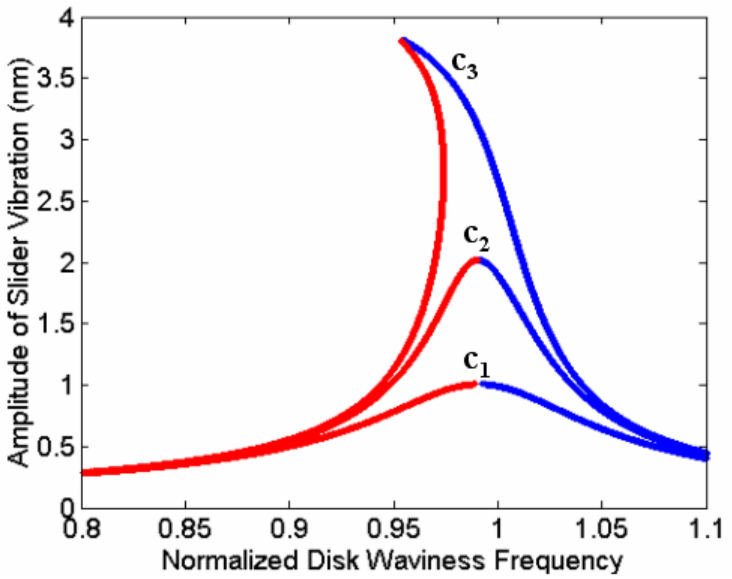

Fig.8 Evolution of the resonance peak computed for three different values of air bearing damping: $c_1 = 0.2$ *N/m/sec,* $c_2 = 0.1$ *N/m/sec and* $c_3 = 0.055$ *N/m/sec*. The numerical parameters are $D = 4nm$, $k = 2.5*10^6$ *N/m,* $H = 8.9*10^{-20}$ *J,* $v = 0.3$ *volts,* $dxdy = 1000\ \mu m^2$.

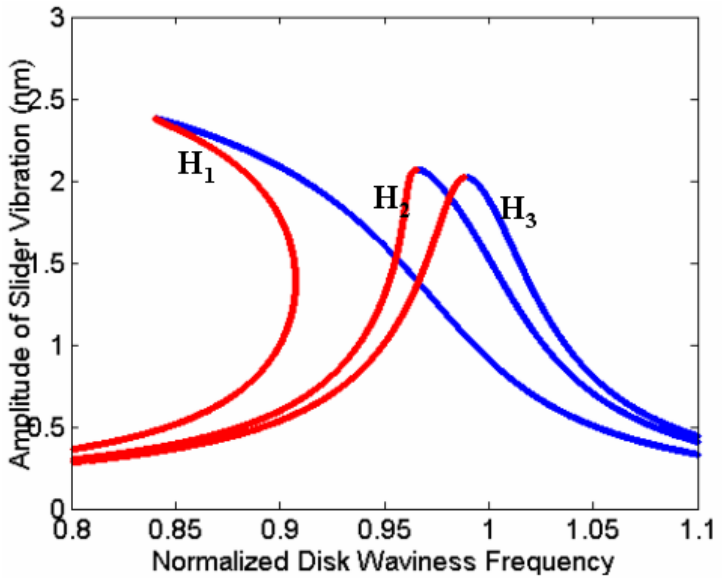

Fig.9 Evolution of the resonance peak computed for three different values of the Hamakar constant: $H_1 = 2.7*10^{-19}$ J, $H_2 = 8.9*10^{-20}$ J and $H_3 = 2.9*10^{-20}$ J. The numerical parameters are $D = 3.8$ nm, $k = 2.5*10^6$ N/m, $c = 0.1$ N/m/sec, $v = 0$ volts, $dxdy = 1000\ \mu m^2$.

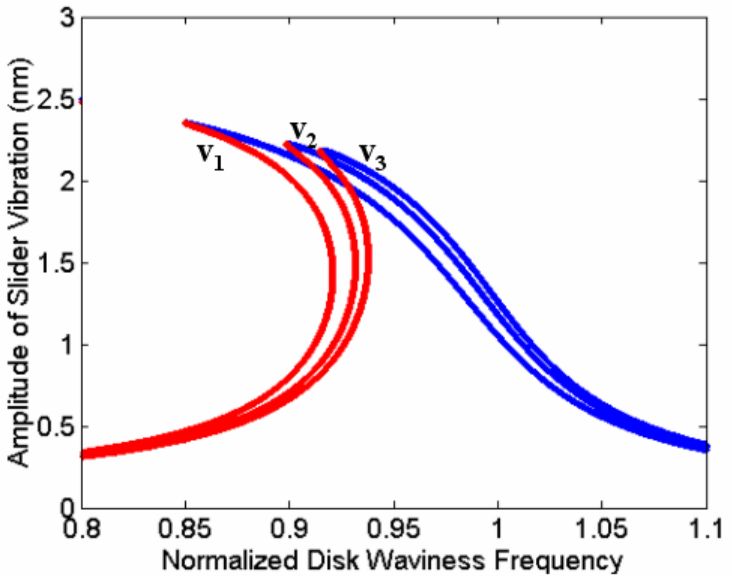

Fig.10 Evolution of the resonance peak computed for three different values of potential difference between the slider and the disk: $v_1 = 0.5$ *volts,* $v_2 = 0.3$ *volts and* $v_3 = 0$ *volts.* The numerical parameters are $D = 3.4$ *nm,* $k = 2.5*10^6$ *N/m,* $c = 0.1$ *N/m/sec,* $H = 8.9*10^{-20}$ *J, dxdy =* $1000\ \mu m^2$.

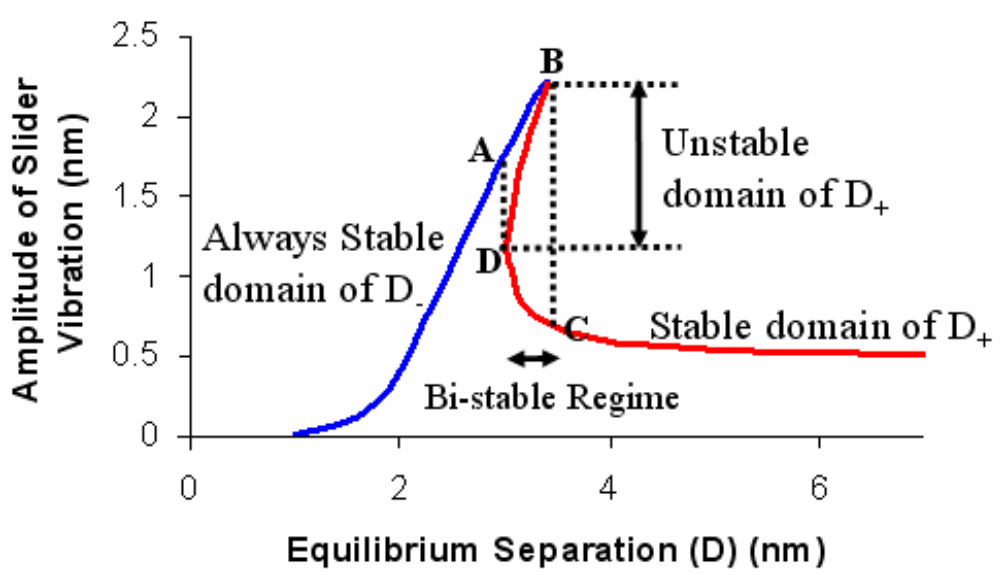

Fig. 11 Variation of the amplitude as a function of the distance, i.e. the approach-retract curve. The numerical parameters are *k = 2.5*106 N/m, c = 0.1 N/m/sec, u = 0.9, H = 2.9*10-20 J, and v = 0.0 volts.* The curve exhibits a hysteretic cycle (ABCD) due to the nonlinear force that characterizes bifurcations from a mono-stable to a bi-stable state.